Analyzing Decision Polygons of DNN-based Classification Methods

Jongyoung Kim, Seongyoun Woo, Wonjun Lee, Donghwan Kim and Chulhee Lee
Department of Electrical and Electronic Engineering, Yonsei University,
134 Shinchon-Dong, Seodaemun-Gu, Seoul, Republic of Korea

Keywords: Decision Polygon, ReLU, Convolutional Neural Networks, Decision Boundary.

Abstract: Deep neural networks have shown impressive performance in various applications, including many pattern recognition problems. However, their working mechanisms have not been fully understood and adversarial examples indicate some fundamental problems with DNN-based classification methods. In this paper, we investigate the decision modeling mechanism of deep neural networks, which use the ReLU function. We derive some equations that show how each layer of deep neural networks expands the input dimension into higher dimensional spaces and generates numerous decision polygons. In this paper, we investigate the decision polygon formulations and present some examples that show interesting properties of DNN based classification methods.

1 INTRODUCTION

Deep neural networks (DNN) have been successfully applied in various computer vision and pattern recognition problems, which include speech recognition (Sainath, 2015, Amodei, 2016), object recognition (Ouyang, 2015, Wonja, 2017, Girshick, 2014), image processing (Jin, 2017), medical imaging (Gibson, 2018), and super-resolution. Although the DNN-based methods have substantially outperformed conventional methods in many fields, the understanding of their working models is rather limited (Radford, 2015, Yang, 2017, Zeiler, 2014, Yosinski, 2014, 2015, Koushik, 2016, Szegedy, 2013, Mallat, 2016).

In (Zeiler, 2014), a visualization method was proposed, which can provide some insight into the intermediate feature spaces and classification operation. Also, it is observed that the first-layer features may not be specific to a particular task, but can be transferable to other tasks (Yosinski, 2014). In (Yosinski, 2015), some visualization tools were proposed, which may provide some insight and understanding of DCN working mechanisms. In (Koushik, 2016), the author presented some analyses of DCN operations in the form of a framework.

The paper is organized as follows: In Section 2 we explain how filter banks project the space into a higher dimension space and the ReLU function creates a higher dimensional structure. Section 3 describes the decision polygon generation when the ReLU function is used along with some properties of the decision polygons. Section 4 investigates adversarial images based on the decision polygons and subspaces. Conclusions are drawn in Section 5.

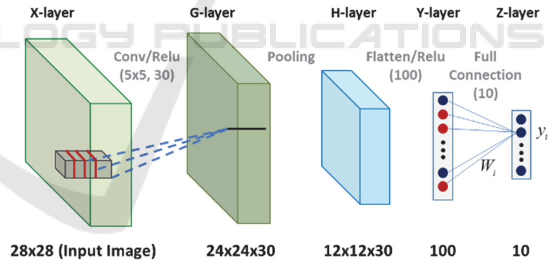

Figure 1: DCN-based classification method for the MNIST data (softmax operation is not shown).

2 SPACE DIVISION BY FILTER BANK

Fig. 1 shows a convolutional neural networks for the MNIST dataset. First, thirty 2-dimensional FIR filters (filter banks) are applied to the input hidden layers. In this case, the FIR filters are square (e.g., 5x5). The number of filters exceeds the number of pixels of the window, though it can be the same as or smaller than the number of pixels of the window. The ReLU function is defined as follows:

Kim, J., Woo, S., Lee, W., Kim, D. and Lee, C.
Analyzing Decision Polygons of DNN-based Classification Methods.
DOI: 10.5220/0009888203460351
In *Proceedings of the 17th International Conference on Informatics in Control, Automation and Robotics (ICINCO 2020)*, pages 346-351
ISBN: 978-989-758-442-8

$$f(x) = max(0, x) \, .$$

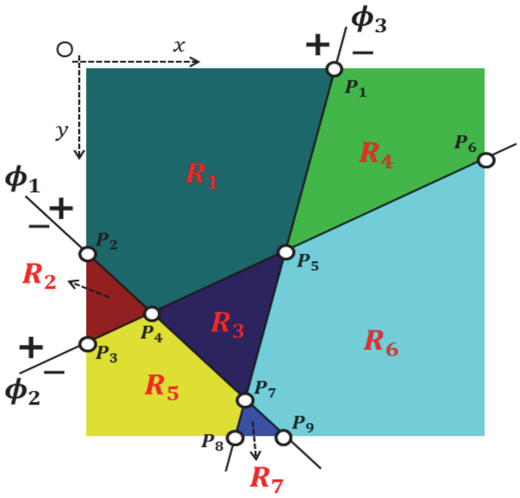

Figure 2: Three filters in the 2 dimensional space.

Fig. 2 illustrates how multiple filters with the ReLU function perform non-linear mapping. In Fig. 2, there are three filters in the 2 dimensional input space, which map the input space into a higher space (3 dimensional space). The three filters can be expressed as follows:

$$X \bullet \phi_1 + c_1 = 0$$
$$X \bullet \phi_2 + c_2 = 0$$
$$X \bullet \phi_3 + c_3 = 0$$

where ϕ_1, ϕ_2, ϕ_3 and X are two-dimensional vectors. In general, the three equations represent planes or hyper-planes in high dimensional spaces and ϕ_1, ϕ_2, ϕ_3 are the normal vectors to the planes.

The three filters divide the input space into seven regions (Fig. 2). One region (R7) is mapped to a point in the 3-dimensional space (Fig. 3a). Two regions (R5, R6) are mapped into lines in the 3-dimensional space (Fig. 3b). Three regions (R2, R3, R4) are mapped into 2-dimensional polygons (Fig. 3c).

In region R7, we have the following relationships:

$$X \bullet \phi_1 + c_1 < 0, X \bullet \phi_2 + c_2 < 0, X \bullet \phi_3 + c_3 < 0.$$

In region R5,

$$X \bullet \phi_1 + c_1 < 0, X \bullet \phi_2 + c_2 < 0, X \bullet \phi_3 + c_3 > 0.$$

In region R1, we have the following:

$$X \bullet \phi_1 + c_1 > 0, X \bullet \phi_2 + c_2 > 0, X \bullet \phi_3 + c_3 > 0.$$

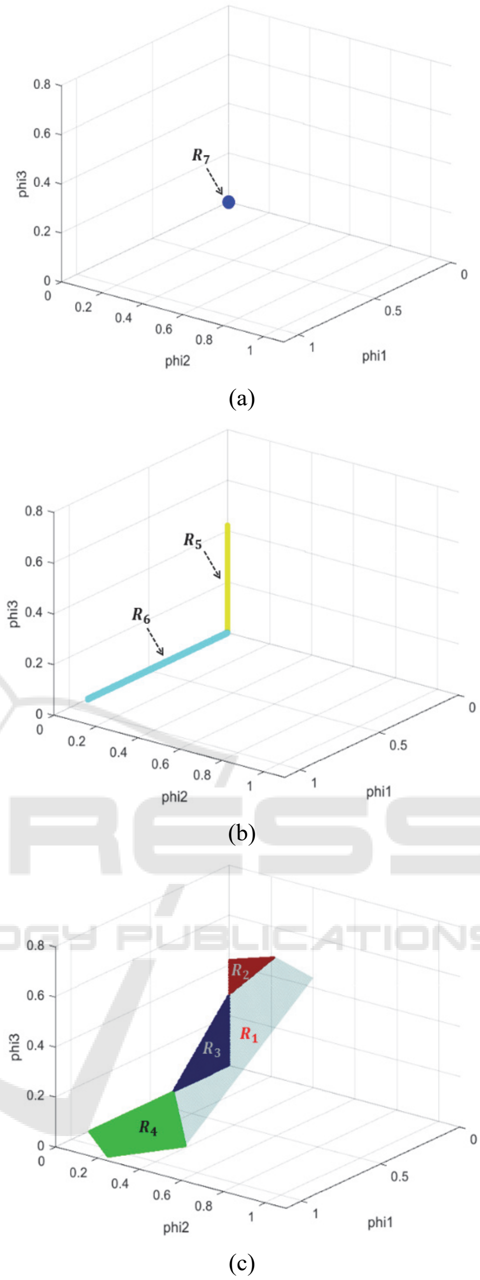

Figure 3: Non-linear mapping of the ReLU function. (a) Region 7 is mapped into a point, (b) Regions 5 and 6 are mapped into lines, (c) three regions (R2, R3, R4) are mapped into 2-dimensional polygons.

For the other regions, we can derive similar relationships. It can be seen that a polygon in the original input space can be mapped into a polygon in the same dimensional space or a lower dimensional space. Also, a polygon may have a lower degree of freedom in the expanded space. For example, a triangle can be mapped into a point, a line or a triangle in the expanded space when ReLU is used in convolutional neural networks. It is also noted that a polygon in the original space never increase its dimension. For example, a triangle in the original space cannot be mapped into a pyramid or a higher dimensional polygon. At most, they can retain their original dimension in a higher dimensional space. However, as we can construct a three dimensional object by folding a paper, the non-linear function of CNN allows the original space mapped into a higher dimensional object through the non-linear function. Nevertheless, the local dimension in the higher space is always the same as in the original space. For example, although a folded paper can make a 3D structure, locally it is always a 2D structure (plane).

3 DECISION POLYGONS OF DNN WITH RELU

In deep convolutional networks, another filter bank or full connection layer can be applied to the output images. These operations can be viewed as a projection on a vector and all the points on a plane that is normal to the vector will be mapped into a single value (Fig. 4a). For example, if we move on the dotted line in the expanded space (Fig. 4a), the projection value on the vector will remain the same. Consequently, the decision boundary will be locally linear and the corresponding decision boundary in the original space will be also locally linear (Fig. 4b). For example, the decision boundary in region R4 is locally linear (a line normal to $\alpha_1\phi_1 + \alpha_2\phi_2$) and the corresponding decision boundary in region R4 of the original input space is locally linear (a line normal to $\alpha_1\phi_1 + \alpha_2\phi_2$).

The max-pooling operation can be also viewed as dividing a space into several subspaces. For example, in 2 by 2 max-pooling, the maximum of four values is selected. Consider the G-layer in Fig. 1. Without loss of generality, we may skip the ReLU operation since the operation doesn't change the output of the max-pooling operation. Thus, the max-pooling operation chooses the maximum value among the four values $(G_0 \bullet X_{28\times28}, G_1 \bullet X_{28\times28}, G_2 \bullet X_{28\times28}, G_3 \bullet X_{28\times28})$:

$$Choose\ G_i \bullet X_{28\times28}\ \ if\ G_i \bullet X_{28\times28} > G_j \bullet X_{28\times28}$$
$$(i,j = 0,..,3; i \neq j).$$

The four vectors (G_0, G_1, G_2, G_3) represent hyper-planes in the input space and the inequality equations divide the input space into a number of polygons. Therefore, the max-pooling operation will divide the input space into a number of subspaces and all the points of a subspace will have the same output for the max-pooling operation. In other words, for each point ($X_{28\times28}$) of a subspace, $G_i \bullet X_{28\times28}$ will be the maximum.

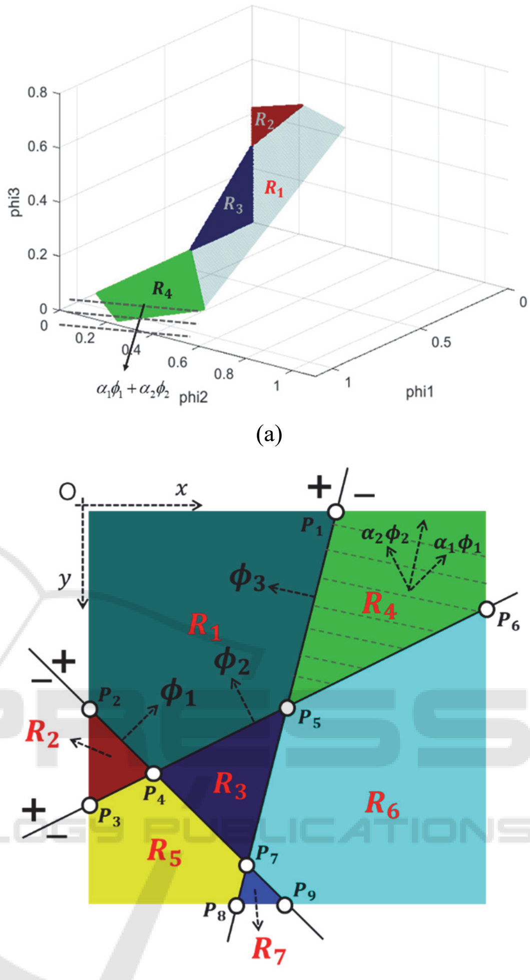

(b)

Figure 4: Decision boundary formation in the expanded space (a) and in the original space (b).

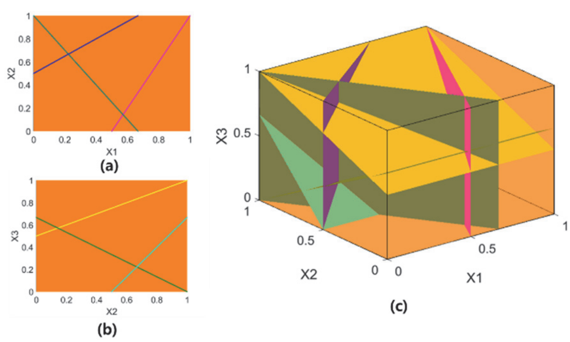

Figure 5: Space division into polygons. (a) three lines divide the $x_1 - x_2$ space into 6 regions, (b) the same three lines divide the $x_2 - x_3$ space into 6 regions, (c) corresponding 3D volume divisions (polygons).

Eventually, the original space will be divided into a number of decision polygons and all the points within the same polygon will be classified as the same class when DNN with ReLU is used as a classifier (Fig. 5). It is noted that the input dimension is very large in typical problems and the planes defined by the filter banks of the first layer are parallel to most of the axes since the filter banks are highly localized. The number of decision polygons may exceed the number of training samples. In the MNIST dataset, the number of training samples is 60,000 and the number of test samples is 10,000. Table I shows the number of samples of decision polygons. After training the DCN of Fig. 1 using the 60,000 training samples, we investigated the decision polygons occupied by the training and test samples. It is found that 69,924 decision polygons are occupied by a single sample. Only 34 decision polygons contain more than one sample. Also, many decision polygons may be unoccupied.

Table 1: Number of samples within decision polygons.

No. samples per polygon	No. polygons
1	69924
2	29
3	3
4	1
5	1

Recently, a number of DCN-based super resolution methods have been proposed (Kim, 2016, Lim, 2017, Zhang, 2018, Wang, 2018), which showed noticeably improved performance compared to conventional super-resolution techniques. When DCN-based super resolution methods use the ReLU function, the filter banks and full-connection layers also divide the input space (receptive field) into a large number of polygons. In this case, each image patch can be considered as a point in the input space and it will belong to one of the polygons. We investigated over 22,000 image patches and found that every image patch belonged to a different polygon. In other words, it is observed that the polygons generated by a DCN-based super resolution method with ReLU are occupied by at most one sample.

4 DECISION BOUNDARY MARGIN OF DNN WITH RELU

4.1 Adversarial Images

Recently, a strange behavior of DNN-based classifier has been reported (Szegedy, 2013). A slightly modified image may be misclassified (Fig. 6) and such adversarial images can be easily generated to fool DNN-based classifiers. Also, one can easily fool DNN-based classifiers to misclassify meaningless images with certainty (Fig. 7).

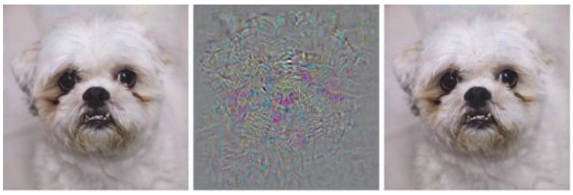

(a) (b) (c)

Figure 6: (a) original image, (b) difference image, (c) modified image.

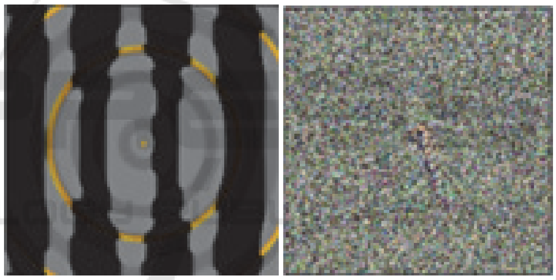

(a) (b)

Figure 7: (a) classified as king penguin, (b) classified as cheetah.

4.2 Mathematical Analyses on DNN-based Classifiers

In general, the layer dimensions are significantly larger than the input dimension. In Fig. 1, the input dimension is 784 (28 x 28), the G-layer dimension is 17280, the H-layer dimension is 4320 and the Y-layer dimension is 100, the Z-layer (output layer) dimension is 10:

$$X = [x_1, x_2, \ldots, x_{784}]^T,\ G = [g_1, \ldots, g_{17280}]^T,$$
$$H = [h_1, \ldots, h_{4320}]^T,\ Y = [y_1, \ldots, y_{100}]^T,$$
$$Z = [z_1, \ldots, z_{10}]^T.$$

In other words, an input image is viewed as a point in the 784 dimensional space. We can compute the gradients of each layer. The Z-layer gradients with respect to the X-layer and the Y-layer are given by

$$\nabla^X z_i \equiv \frac{\partial z_i}{\partial X} = \left[\frac{\partial z_i}{\partial x_1}, \dots, \frac{\partial z_i}{\partial x_{784}}\right]^T,$$
$$\nabla^Y z_i \equiv \frac{\partial z_i}{\partial Y} = \left[\frac{\partial z_i}{\partial y_1}, \dots, \frac{\partial z_i}{\partial y_{100}}\right]^T, (i = 1 \sim 10).$$

Although the Y-layer dimension is 100, the number of linearly independent vectors that can affect the outputs (z_i) is 10, which is equal to the number of classes. The remaining 90 vectors that are normal to the 10 vectors don't affect the output values (z_i). We define the subspace spanned by the 10 vectors (φ_i^k) as a relevant subspace (S_{relSub}^k) and the subspace spanned by the 90 vectors as an irrelevant subspace (S_{irrSub}^k):

$$S_{relSub}^k = span(\varphi_i^k)$$
$$S_{irrSub}^k = span(\psi_j^k) \; (\varphi_i^k \bullet \psi_j^k = 0).$$

where i and j are vector indexes, and k is the layer index. In each layer, the layer space can be divided into relevant and irrelevant subspaces and the dimension of relevant space can't exceed the number of classes. When a sample moves in irrelevant subspaces, all the output values (z_i, i = 0,..,9) remain the same. Consequently, one can almost unlimitedly generate equivalent images, many of which can be meaningless images.

In the previous section, it is shown that DNN-based classifiers divide the input space into a large number of decision polygons and each decision polygon is very sparsely populated. In other words, most polygons may be unoccupied by training or test samples It is observed that the margin between a sample and the boundaries of decision polygons is very small (Woo, 2018). Fig. 8 shows the within-class MSE histogram and the between-class MSE histogram, which indicate the margins between samples and the boundaries of decision polygons.

5 CONCLUSIONS

In this paper, we investigate the working mechanism of DNN-based classifiers. When filter bank or full-connection layers are applied along with the ReLU function to a layer, the layer space is divided into a number of polygons. Eventually, the input space is divided into a large number of decision polygons. Several interesting properties are observed. A vast majority of decision polygons are occupied by a single sample and the margin between the sample and the boundaries of the decision polygon is very small. In the layer space, the dimension of the relevant subspace exceeds the dimension of the irrelevant subspace in most cases. Consequently, in current structures of DNN-based classifiers, it is difficult to prevent misclassification of adversarial images. In particular, to effectively handle adversarial images, new type of DNN-based methods may be needed, which provide larger margins between samples and the boundaries of decision polygons and adequate controls of irrelevant subspaces.

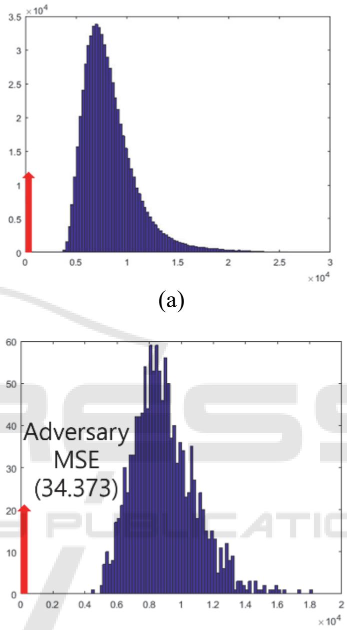

(a) (b)

Figure 8: (a) within-class MSE histogram, (b) between–class MSE histogram.

ACKNOWLEDGEMENTS

This research was supported by Basic Science Research Program through the National Research Foundation of Korea (NRF) funded by the Ministry of Education, Science and Technology (2017R1D1A1B03036172).

REFERENCES

Sainath, T. N., Kingsbury, B., Saon, G., Soltau, H., Mohamed, A. R., Dahl, G., & Ramabhadran, B. (2015). Deep convolutional neural networks for large-scale speech tasks. *Neural Networks*, *64*, 39-48.

Ouyang, W., Wang, X., Zeng, X., Qiu, S., Luo, P., Tian, Y., & Tang, X. (2015). Deepid-net: Deformable deep convolutional neural networks for object detection. In *Proceedings of the IEEE conference on computer vision and pattern recognition* (pp. 2403-2412).

Jin, K. H., McCann, M. T., Froustey, E., & Unser, M. (2017). Deep convolutional neural network for inverse problems in imaging. *IEEE Transactions on Image Processing*, *26*(9), 4509-4522.

Woo, S., & Lee, C. L. (2018, August). Decision boundary formation of deep convolution networks with relu. In *2018 IEEE 16th Intl Conf on Dependable, Autonomic and Secure Computing, 16th Intl Conf on Pervasive Intelligence and Computing, 4th Intl Conf on Big Data Intelligence and Computing and Cyber Science and Technology Congress (DASC/PiCom/DataCom/CyberSciTech)* (pp. 885-888). IEEE.

Wojna, Z., Gorban, A. N., Lee, D. S., Murphy, K., Yu, Q., Li, Y., & Ibarz, J. (2017, November). Attention-based extraction of structured information from street view imagery. In *2017 14th IAPR International Conference on Document Analysis and Recognition (ICDAR)* (Vol. 1, pp. 844-850). IEEE.

Gibson, E., Li, W., Sudre, C., Fidon, L., Shakir, D. I., Wang, G., ... & Whyntie, T. (2018). NiftyNet: a deep-learning platform for medical imaging. *Computer methods and programs in biomedicine*, *158*, 113-122.

Amodei, D., Ananthanarayanan, S., Anubhai, R., Bai, J., Battenberg, E., Case, C., ... & Chen, J. (2016, June). Deep speech 2: End-to-end speech recognition in english and mandarin. In *International conference on machine learning* (pp. 173-182).

Girshick, R., Donahue, J., Darrell, T., & Malik, J. (2014). Rich feature hierarchies for accurate object detection and semantic segmentation. In *Proceedings of the IEEE conference on computer vision and pattern recognition* (pp. 580-587).

Radford, A., Metz, L., & Chintala, S. (2015). Unsupervised representation learning with deep convolutional generative adversarial networks. *arXiv preprint arXiv:1511.06434*.

Yang, H. F., Lin, K., & Chen, C. S. (2017). Supervised learning of semantics-preserving hash via deep convolutional neural networks. *IEEE transactions on pattern analysis and machine intelligence*, *40*(2), 437-451.

Zeiler, M. D., & Fergus, R. (2014, September). Visualizing and understanding convolutional networks. In *European conference on computer vision* (pp. 818-833). Springer, Cham.

Yosinski, J., Clune, J., Bengio, Y., & Lipson, H. (2014). How transferable are features in deep neural networks?. In *Advances in neural information processing systems* (pp. 3320-3328).

Yosinski, J., Clune, J., Nguyen, A., Fuchs, T., & Lipson, H. (2015). Understanding neural networks through deep visualization. *arXiv preprint arXiv:1506.06579*.

Koushik, J. (2016). Understanding convolutional neural networks. *arXiv preprint arXiv:1605.09081*.

Szegedy, C., Zaremba, W., Sutskever, I., Bruna, J., Erhan, D., Goodfellow, I., & Fergus, R. (2013). Intriguing properties of neural networks. *arXiv preprint arXiv:1312.6199*.

Mallat, S. (2016). Understanding deep convolutional networks. *Philosophical Transactions of the Royal Society A: Mathematical, Physical and Engineering Sciences*, *374*(2065), 20150203.

Kim, J., Kwon Lee, J., & Mu Lee, K. (2016). Accurate image super-resolution using very deep convolutional networks. In *Proceedings of the IEEE conference on computer vision and pattern recognition* (pp. 1646-1654).

Lim, B., Son, S., Kim, H., Nah, S., & Mu Lee, K. (2017). Enhanced deep residual networks for single image super-resolution. In *Proceedings of the IEEE conference on computer vision and pattern recognition workshops* (pp. 136-144).

Zhang, Y., Li, K., Li, K., Wang, L., Zhong, B., & Fu, Y. (2018). Image super-resolution using very deep residual channel attention networks. In *Proceedings of the European Conference on Computer Vision (ECCV)* (pp. 286-301).

Wang, X., Yu, K., Wu, S., Gu, J., Liu, Y., Dong, C., ... & Change Loy, C. (2018). Esrgan: Enhanced super-resolution generative adversarial networks. In *Proceedings of the European Conference on Computer Vision (ECCV)* (pp. 0-0).